GNSS/LiDAR Integration Aided by Self-adaptive Gaussian Mixture Models in Urban Scenarios: An Approach Robust to Non-Gaussian Noise

Weisong Wen, Xiwei Bai, Li-Ta Hsu*
The Hong Kong Polytechnic University
Kowloon, Hong Kong
Correspondence: lt.hsu@polyu.edu.hk

Tim Pfeifer
Chemnitz University of Technology
Chemnitz, Germany
tim.pfeifer@etit.tu-chemnitz.de

***Abstract*—Accurate and globally referenced positioning is crucial to autonomous systems with navigation requirements, such as unmanned aerial vehicles (UAV) and autonomous driving vehicles (ADV). GNSS/LiDAR integration is a popular sensor pair that can provide outstanding positioning performance in open areas. However, the accuracy is significantly degraded in urban canyons, due to the excessive unmodeled non-Gaussian GNSS outliers caused by multipath effects and none-line-of-sight (NLOS) receptions. As a result, the violation of the Gaussian assumption can severely distort the sensor fusion process, such as the extended Kalman filter (EKF). To mitigate the effects of these non-Gaussian GNSS outliers, this paper proposes to leverage the Gaussian mixture model (GMM) to describe the potential noise of GNSS positioning and apply it to further sensor fusion. Instead of relying on excessive offline parameterization and tuning, the parameters of the GMM are estimated simultaneously based on the residuals of the GNSS measurements using an expectation-maximization (EM) algorithm. Then the state-of-the-art factor graph optimization (FGO) is applied to integrate the GNSS positioning and LiDAR odometry based on the estimated GMM. The experiment in a typical urban canyon is conducted to validate the performance of the proposed method. The result shows that the GMM can effectively mitigate the effects of GNSS outliers and improves positioning performance.**

Keywords—GNSS; LiDAR; Positioning; Non-Gaussian noise; Factor graph optimization; Gaussian mixture models, Urban canyon

I. INTRODUCTION

Global navigation satellite systems (GNSS) [1] are one of the indispensable sensors to provide global referenced positioning for autonomous systems, such as unmanned aerial vehicles (UAV) [2] and autonomous driving vehicles (ADV) [3]. GNSS can obtain satisfactory accuracy in open areas with an accuracy of ~5 meters. However, the performance can be significantly degraded in urban canyons due to the notorious multipath effects and none-line-of-sight (NLOS) receptions [1]. As a result, more than 50 meters of positioning error can be caused accordingly in urban canyons [4]. Light detection and ranging (LiDAR) based simultaneous localization and mapping (SLAM) [5] is a well-known technology to provide relative positioning due to its robustness against the illumination, compared with the visual-based SLAM. The major principle of LiDAR-based SLAM is to track the motions between consecutive frames of point clouds to obtain accurate relative positioning over a short period. However, its performance is subject to drift over time [6]. Moreover, the LiDAR SLAM can fail in the open area with limited features and only relative positioning is provided. Due to the complementariness between GNSS and LiDAR positioning, a lot of researches [7-11] is investigated to integrate the GNSS and LiDAR to achieve long-term autonomy. Decent performance can be obtained by GNSS/LiDAR integration in the open area when the GNSS positioning is satisfying and the sensor error is well distributed as Gaussian noise. Unfortunately, in urban canyons, the noise model of GNSS does not always subject to Gaussian distribution [12], due to the multipath and NLOS effects causing numerous unexpected outliers. The performance of popular filtering-based [13] methods (e.g. extended Kalman filter [14]), relies on the assumption that the sensor noise follows a Gaussian distribution. Recently, factor graph optimization (FGO) [15] is proposed to integrate information from multiple sensors via optimization. Interestingly, according to our recent research [16], we found that the optimization-based [9] sensor fusion using factor graph [17] outperforms the conventional filtering based methods, due to the multiple iterations and re-linearization process in FGO. However, the existing factor graph-based optimization still relies on the Gaussian assumption, although it is more resilient against the outlier measurements. In short, excessive unpredictable and non-Gaussian GNSS outliers are still major problems of GNSS/LiDAR integration in urban canyons.

To mitigate the effects of NLOS receptions and multipath effects, numerous researches are studied, such as the 3D mapping aided GNSS (3DMA GNSS) [18, 19], the 3D LiDAR aided GNSS positioning [20-24] and the camera aided GNSS positioning [25, 26]. However, these methods rely heavily on the availability of environment descriptions, such as 3D building models or perceived sky view. Moreover, these solutions still cannot essentially cope with the non-Gaussian properties of GNSS. Recently, the Gaussian mixture model (GMM) is theoretically investigated in [27] to model the non-Gaussian noise of loop-closure in SLAM.

978-1-7281-0244-3/20/$31.00 ©2020 IEEE

However, only the max-mixture [27] model is employed to approximate the actual GMM. To solve the problem of arbitrary error distribution of sensor noise in factor graph-based sensor fusion, the mixture of Cauchy distribution is investigated in [28] and improved performance is obtained. Unfortunately, only limited evaluation is provided. It is still an open task to exploit its potential in multi-sensor fusion applications. In brief summary, the works in [27] and [28] have theoretically validated the feasibility of modeling the sensor noise with non-Gaussian distribution which can be applied to the FGO accordingly.

The authors of [12, 29, 30] recently proposed a set of algorithms that address the strong non-Gaussian properties of pseudorange measurements with adaptive GMMs. Firstly described in [30], they solve the single point positioning (SPP) problem using FGO and an implicit expectation-maximization (EM) approach to adapt the sensor model during the optimization. In [12] the implicit EM is made explicit by performing the GMM estimation separately from the standard FGO. Based on the pseudorange measurement residuals, a mixture model with a fixed number of components is estimated with EM. In the most recent work [29] the EM is replaced by Bayesian inference which allows the online adaption of the number of GMM components. The applied variational Bayesian inference makes the GMMs estimation more robust with the price of increased computation time. For efficiency, we prefer the EM approach [12] within this paper.

In parallel, the authors of [31, 32] proposed a similar approach that is applied to precise point positioning (PPP) for airplane applications. They also use VBI as well as sampling-based methods and mainly address batch processing for offline estimation problems. All of these adaptive FGO approaches are able to reduce the NLOS induced localization errors by a magnitude, which shows the high potential of adaptive GMMs in sensor fusion. However, the methods from both groups rely on a good initial guess of the estimated states to calculate the residuals and their corresponding distribution. In other words, they rely on the assumption that the residuals can effectively represent the actual error distribution. If this condition holds in a multi-sensor setup is still an open question. Existing publications also lack an experimental evaluation outside the specific pseudorange domain.

Inspired by the efforts of both groups, we go one step further and apply the adaptive GMM approach to the common multi-sensor GNSS/LiDAR integration problem. Within this work, we want to show how the approach can be applied to robustly localize in the dense urban canyons of Hong Kong. We not only analyze the localization performance, we investigate also if the model assumption of this approach holds under these harsh conditions. The proposed GNSS/LiDAR integration framework can efficiently integrate diverse positioning sources with GMM, such as visual odometry, which we believe is also one contribution of this paper.

The remainder of this paper is structured as follows. An overview of the proposed method is given in Section II. Section III presents the GMM and its parameter estimation via the EM algorithm. The GNSS/LiDAR integration is introduced in Section IV before the experimental evaluation is presented in Section V. Finally, the conclusions and future work are drawn in Section VI.

II. Overview of the Proposed Method

The overview of the proposed GNSS/LiDAR integration is shown in Fig. 1. The inputs of the system include the 3D point clouds (P_t) from 3D LiDAR and GNSS measurements ($Z_{gnss,i}$). Firstly, point cloud registration is performed to estimated motion between consecutive frames of 3D laser scans using NDT [33]. Then the LiDAR odometry factor (r_i^{LiDAR}) is derived to represent the estimated relative pose in the FGO. Secondly, the loosely-coupled GNSS factor (r_i^{gnss}) is derived based on the positioning information from the GNSS receiver. Thirdly, optimization is performed to initialize the system states. Then the residuals of all the historical GNSS measurements are calculated based on the estimated states. Fourthly, the parameters of the GMM is estimated based on the residuals using an EM algorithm. Finally, the estimated GMM is fed back to the FGO and the states of the vehicle are obtained by solving the factor graph again.

The major contributions of this paper are listed as follows:

(1) This paper proposes a state-of-the-art adaptive GMM to model the GNSS measurements in urban canyons. Moreover, the parameters of the GMM are estimated online without prior knowledge.

(2) This paper applies the GMM to the GNSS/LiDAR integration using FGO to mitigate the impacts of the GNSS outliers.

(3) This paper evaluates the performance of the proposed GNSS/LiDAR integration using a real-world dataset, recorded in the urban canyons of Hong Kong

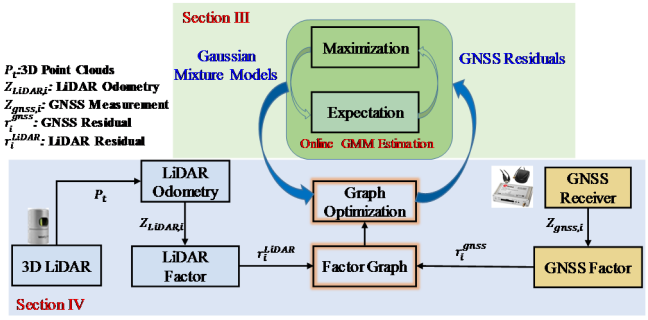

Fig. 1. Illustration of the proposed GNSS/LiDAR integration framework aided by GMM.

III. Gaussian Mixture Models for GNSS Measurement

This section presents the formulation of GMM in FGO optimization. Then the estimation of the parameters of GMM is presented subsequently.

A. Gaussian Mixture Models in Factor Graph Optimization

Even for the state-of-the-art FGO in sensor fusion [15], the assumption that the sensor error is distributed according to a Gaussian distribution is mandatory. Unfortunately, there are a lot of scenarios, where the sensor noise is multi-modal and

single modal distribution cannot represent it effectively. A Gaussian mixture model is a promising approach for these cases. With the weighted sum of different Gaussian components, the GMM can describe the majority of non-Gaussian distributions.

Following our previous work in [12], the GMM can be denoted as follows:

$$P(z_i|x_i) = \sum_j w_j \cdot \mathcal{N}(z_i; \mu_j, \sigma_j^2) \tag{1}$$

Where z_i denotes the measurements (e.g. the GNSS measurements), w_j represents the weighting of the Gaussian component j and μ_j and σ_j represent the corresponding mean and standard deviation, respectively.

The FGO [15] formulates the sensor fusion as a non-linear least squares problem as follows:

$$\boldsymbol{X}^* = \arg\max_{\boldsymbol{X}} P(\boldsymbol{X}|Z) \tag{2}$$

Where $\boldsymbol{X} = \{x_1, x_2, x_3, \dots, x_i\}$ is a set of states to be estimated, Z is a set of measurements from the first epoch to the current epoch and $\boldsymbol{X}^*$ denotes the optimal set of states after the FGO. Since each measurement is considered as a factor in FGO, the problem (2) can be formulated as the product of conditional probabilities as follows [12, 15]:

$$P(\boldsymbol{X}|Z) \propto \prod_i P(z_i|x_i) \tag{3}$$

Where x_i denotes the state associated with the measurement z_i. In fact, $P(z_i|x_i)$ is considered as a factor and the subscript i denotes the index of the factor in FGO. The formulation (2) can be transformed as follows using the negative logarithm:

$$\boldsymbol{X}^* = \arg\min_{\boldsymbol{X}} \sum_i -\ln P(z_i|x_i) \tag{4}$$

For a sum of Gaussian with N components representing the measurement z_i, the conditional probability can be formulated as follows [12]:

$$P(z_i|x_i) \propto \sum_{j=1}^{N} c_j \cdot \exp\left(-\frac{1}{2}\left\|\Im_j^{\frac{1}{2}}(e_i - \mu_j)\right\|^2\right) \tag{5}$$

$$\text{with } c_j = w_j \cdot \det\left(\Im_j^{\frac{1}{2}}\right) \text{ and } \Im_j^{\frac{1}{2}} = \Sigma_j^{-\frac{1}{2}} \tag{6}$$

Where the e_i denotes the residual of measurement z_i and the $\Im_j$ is the information matrix corresponding to the measurement e_i. It's square root can be calculated using the Cholesky decomposition of the inverse covariance matrix Σ_j. Therefore, the sensor fusion problem with GMM can be formulated by integrating the (5) to (4).

For the Gaussian case, formulation (4) can be easily transformed into a standard least-squares problem [15]. To represent the GMM in the FGO, the authors of [34] proposed the max-mixture algorithm where the GMM is described using the Gaussian component with maximum probability. Therefore, only a approximation of the exact distribution is obtained. The exact implementation of non-Gaussian distributions inside the FGO is proposed recently in [28]. The authors of [12] shows its feasibility for GMMs in GNSS single point positioning. In this paper, we apply this exact sum-mixture approach to implement the GMM into the FGO. Based on the work in [28], the FGO problem with explicit GMM can be formulated as follows:

$$\boldsymbol{X}^* = \arg\min_{X} \sum_i \left\| \sqrt{-\ln\left(\frac{P(z_i|x_i)}{\gamma_s}\right)} \right\|^2 \tag{7}$$

$$\text{with } \gamma_s \geq \max_i(P(z_i|x_i))$$

Where γ_s is a normalization constant [12] to keep the negative log-likelihood positive. We set γ_s as $\sum_j c_j$ in this paper. We can obtain the following integrated formulation by pushing the (5) inside the (7):

$$\boldsymbol{X}^* = \arg\min_{X} \sum_i \left\| \sqrt{-\ln\left(\frac{\sum_{j=1}^{N} c_j \cdot \exp\left(-\frac{1}{2}\left\|\Im_j^{\frac{1}{2}}(e_i-\mu_j)\right\|^2\right)}{\gamma_s}\right)} \right\|^2 \tag{8}$$

Therefore, the optimal set of states $X_{1:t}^*$ can be estimated by solving the FGO with GMM as (8). This is also a general formulation to model arbitrary sensor measurements (e.g. visual odometry) using GMM in FGO.

B. Online Parameters Estimation for Gaussian Mixture Models

The GNSS positioning measurement $Z_{gnss,t}$ is represented as follows:

$$Z_{gnss,i} = \begin{bmatrix} Z_{gnss,i}^E \\ Z_{gnss,i}^N \end{bmatrix} \tag{9}$$

Where the $Z_{gnss,i}^E$ and $Z_{gnss,i}^N$ denote the positioning in the east and north direction at a given epoch i. Be noted that we use the GNSS positioning in ENU [1] coordinate system. As the GNSS positioning error in altitude direction is significantly more unreliable compared with the horizontal positioning. Therefore, we only use the horizontal positioning from GNSS in further integration with LiDAR odometry. Inspired by the work in [12], we use two different GMMs to model the noise model in east and north directions, respectively. This section presents the estimation of the parameters for the GMM in a single dimension, which is, in fact, applicable for both the east and north directions.

The expectation-maximization is an iterative algorithm that can be applied to estimate the maximum-likelihood of parameters (**U**) in statistical models, where the model depends on observed variables (**O**) and a set of hidden variables (**H**). Different from the conventional non-linear least squares problem where the unknown variables can be solved directly, the **O** and **H** cannot be solved directly based on the observed variables. Therefore, we employ an expectation step (E-step) to estimate the hidden variables **H** based on the given initial guess of **U.** Then the estimated **H** is employed to estimate the **U** using a maximization step (M-step). The E-step and the M-step are performed iteratively until the convergence criterion

is satisfied. The parameters for the EM estimation is expressed as follows:

$$\mathbf{O} = \{e_1, e_2, \dots, e_i, \dots e_M\} \tag{10}$$

$$\mathbf{H} = \{\alpha_{ij}\}_{i=1,\dots M; j=1,\dots N;} \tag{11}$$

$$\mathbf{U} = \left\{w_j, \mu_j, \Im_j^{\frac{1}{2}}\right\}_{ij=1,\dots N;} \tag{12}$$

Where M denotes the number of residuals considered for GMM estimation, the e_i represents the residual corresponding to a given measurement z_i which is calculated as follows:

$$e_i = z_i - h(x_i) \tag{13}$$

Where x_i is the state associated with the measurement z_i and $h(*)$ is the observation function. Hidden variable α_{ij} denotes the probability of a given e_i to belong to component j of the estimated GMM. The $\mathbf{U}$ is the parameters for the GMM which is to be estimated.

Based on the residual set $\mathbf{O}$, the E-step can be performed to estimate the hidden variables as follows:

$$\alpha_{ij} = \frac{\mathrm{P}(e_i|w_j,\mu_j,\Im_j^{\frac{1}{2}})}{\sum_{j=1}^{N}\mathrm{P}(e_i|w_j,\mu_j,\Im_j^{\frac{1}{2}})} \tag{14}$$

with

$$\mathrm{P}\left(e_i\middle|w_j,\mu_j,\Im_j^{\frac{1}{2}}\right) = w_j \cdot \det(\Im_j^{\frac{1}{2}}) \exp\left(-\frac{1}{2}\left\|\Im_j^{\frac{1}{2}}(e_i-\mu_j)\right\|^2\right)$$

Therefore, the hidden variables are updated based on the iteration above. Then the M-step is performed to update the parameters of GMM as follows:

$$w_j = \frac{1}{n}\sum_{i=1}^{M}\alpha_{ij} \tag{15}$$

$$\mu_j = \frac{\sum_{i=1}^{M}\alpha_{ij}e_i}{\sum_{i=1}^{M}\alpha_{ij}} \tag{16}$$

$$\Im_j^{\frac{1}{2}T}\Im_j^{\frac{1}{2}} = \left(\frac{\sum_{i=1}^{M}\alpha_{ij}(e_i-\mu_j)(e_i-\mu_j)^T}{\sum_{i=1}^{M}\alpha_{ij}}\right)^{-1} \tag{17}$$

The M-step needs to be conducted for N times to estimate the parameters for all components. Finally, the E-step and the M-step is performed iteratively for several times until the conditional probability $\mathrm{P}\left(e_i\middle|w_j,\mu_j,\Im_j^{\frac{1}{2}}\right)$ change between two iterations is smaller than a given threshold. In this work, the parameters for the GMM are estimated in an online manner.

IV. GNSS/LiDAR Integration Using Factor Graph Optimization with GMM

Fig. 2 shows the proposed factor graph structure for GNSS/LiDAR integration using GMM. The blue circle denotes the LiDAR odometry factor. The green rectangle denotes the GNSS factors with the corresponding noise modeled by GMM (the red shaded eclipse). The state vector in this paper is as follows:

$$\boldsymbol{X} = \{\mathbf{x}_1, \mathbf{x}_2, \dots, \mathbf{x}_i\} \tag{18}$$

$$\mathbf{x}_i = [\mathbf{p}_{b_i}^w, \mathbf{q}_{b_i}^w] \tag{19}$$

Where $\boldsymbol{X}$ denotes the state set from the first to the current epoch. The $\mathbf{x}_i$ represent the state at a given epoch i. Vector $\mathbf{p}_{b_i}^w$ encodes the translation from the world ("w") frame to the body ("b") frame and $\mathbf{q}_{b_i}^w$ the rotation (denoted by a quaternion) from the world ("w") frame to the body ("b") frame, which is expressed using a rotation matrix. The body frame is fixed at the center of the 3D LiDAR in this paper. The world frame is fixed at the starting point in the east, north and up (ENU) [1] coordinate.

The remainder of this section presents the derivation of GNSS factors and LiDAR factor together with their integration.

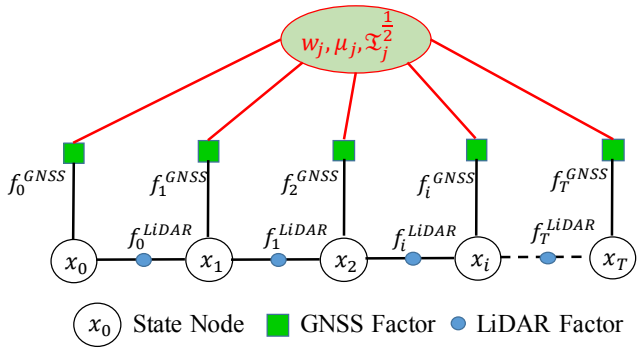

Fig. 2. Illustration of factor graph for the proposed GNSS/LiDAR integration with GMM.

A. GNSS Factor

GNSS observation can provide absolute positioning. The GNSS measurement model is expressed as follows:

$$Z_{gnss,i} = h_{gnss}(\mathbf{x}_i) + n_{gnss} \tag{20}$$

Where n_{gnss} denotes the noise of measurement associated with $Z_{gnss,i}$. Therefore, the residual (r_i^{gnss}) of the GNSS measurement is formulated as follows:

$$r_i^{gnss} = \left\|Z_{gnss,i} - h_{gnss}(\mathbf{x}_i)\right\|_{GMM}^2 \tag{21}$$

$$\text{with } r_i^{gnss} = r_i^{gnss,E} + r_i^{gnss,N}$$

$$r_i^{gnss,E} = \left\|\sqrt{-\ln\left(\frac{\sum_{j=1}^{N} c_j \cdot \exp\left(-\frac{1}{2}\left\|\Im_j^{\frac{1}{2}}\left(e_i^{gnss,E}-\mu_j\right)\right\|^2\right)}{\gamma_s}\right)}\right\|^2 \tag{22}$$

$$r_i^{gnss,E} = \left\|\sqrt{-\ln\left(\frac{\sum_{j=1}^{N} c_j \cdot \exp\left(-\frac{1}{2}\left\|\Im_j^{\frac{1}{2}}\left(e_i^{gnss,N}-\mu_j\right)\right\|^2\right)}{\gamma_s}\right)}\right\|^2 \tag{23}$$

Where $r_i^{gnss,E}$ and $r_i^{gnss,N}$ denote the residuals in the east and north directions, respectively. Be noted that two GMMs are employed to model the positioning noise in east and north

directions, respectively. In this case, the residual for the GNSS measurements modeled with GMM is obtained.

B. LiDAR Factor

LiDAR odometry can provide high-frequency relative positioning by mapping consecutive frames of point clouds [6]. Decent accuracy can only be obtained in a short period due to the inevitably accumulated drift over time. Our GNSS/LiDAR integration can effectively make use of their complementariness.

The principle of LiDAR odometry [35] is to track the transformation between two successive frames of point clouds by matching the two frames of point clouds called reference point cloud and input point cloud in this paper. The matching process is also called point cloud registration. The objective of point cloud registration is to obtain the optimal transformation matrix to match or align the reference and the input point clouds. We employ the normal distribution transform (NDT) [36] to conduct the point cloud registration. The relative transformation $Z_{LiDAR,i}$ derived from the NDT is expressed as follows:

$$Z_{LiDAR,i} = [\mathbf{p}_{b_{i-1}}^{b_i}, \mathbf{q}_{b_{i-1}}^{b_i}] \tag{24}$$

where the $\mathbf{p}_{b_{i-1}}^{b_i}$ and $\mathbf{q}_{b_{i-1}}^{b_i}$ represent the translation and rotation (denoted by a quaternion) between epoch i and epoch $i-1$ in the body frame. Therefore, the residual (r_i^{LiDAR}) of the LiDAR positioning is formulated as follows:

$$r_i^{LiDAR,p} = \left\| \mathbf{p}_{b_i}^{w} - \mathbf{p}_{b_{i-1}}^{w} - \mathbf{q}_{b_{i-1}}^{w} \mathbf{p}_{b_{i-1}}^{b_i} \right\|_{\Sigma_i^p}^2 \tag{25}$$

$$r_i^{LiDAR,q} = \left\| \mathbf{q}_{b_{i-1}}^{w}{}^{-1} \mathbf{q}_{b_i}^{w} \ominus \mathbf{q}_{b_{i-1}}^{b_i} \right\|_{\Sigma_i^q}^2 \tag{26}$$

$$r_i^{LiDAR} = r_i^{LiDAR,p} + r_i^{LiDAR,q} \tag{27}$$

where the $r_i^{LiDAR,p}$ and $r_i^{LiDAR,q}$ denote the residuals for translation and rotation, respectively. Regarding the information for translation (Σ_i^p) and rotation (Σ_i^q), we follow our previous work in [6] where the uncertainty of LiDAR odometry is determined based on the degree of matching. Therefore, the LiDAR factor is derived.

C. Factor Graph Optimization

Based on the derived residuals from the GNSS measurements and LiDAR odometry, the optimal state set can be estimated by solving the following non-linear function:

$$X^* = \arg\min_X \sum_i r_i^{LiDAR} + r_i^{gnss} \tag{28}$$

where the X^* denotes the optimal states set. Regarding the implementation of GMM, we make use of the libRSF[1] [12]. To solve the non-linear optimization problem, we make use of the Levenberg-Marquardt algorithm in Ceres Solver [37].

[1] https://github.com/TUC-ProAut/libRSF

V. Experiment Evaluation

A. Experiment Setup

The proposed method is verified through real road tests in the deep urban canyon of Hong Kong. During the experiment, a u-blox M8T GNSS receiver was used to collect GNSS measurements at a frequency of 2 Hz. The 3D LiDAR sensor (Velodyne 32) was employed to collect raw 3D point clouds at a frequency of 10 Hz. In addition, the NovAtel SPAN-CPT, a GNSS (GPS, GLONASS, and Beidou) RTK/INS (fiber-optic gyroscopes, FOG) integrated navigation system, was used to provide the ground truth of positioning. The gyro bias in-run stability of the FOG is 1 degree per hour and its random walk is 0.067 degree per hour. The baseline between the rover and GNSS base station is about 7 km. All the data were collected and synchronized using the robot operation system (ROS) [38]. The coordinate systems between all the sensors were calibrated before the experiment. The sensor setup is shown in Fig. 3. Fig. 3-(a) shows a snapshot with high-rising buildings on the double sides which is challenging for GNSS solutions. Fig. 3-(b) shows a snapshot with numerous moving objects, which is challenging for LiDAR odometry.

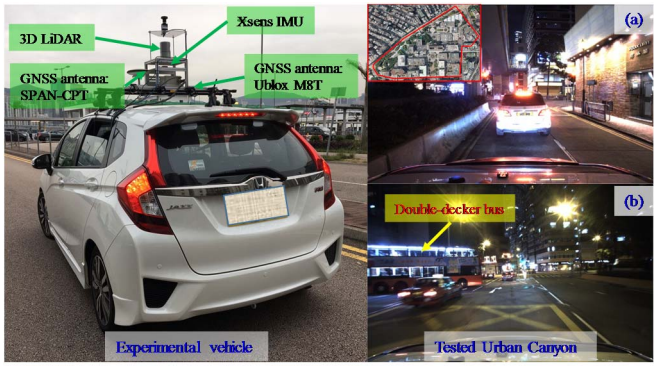

Fig. 3. Illustration of the sensor setup and the tested scenario.

To verify the performance of the proposed method, several methods are compared.

(1) **GNSS**: GNSS standalone positioning provided by the u-blox receiver.

(2) **LIO**: positioning from LiDAR odometry.

(3) **GNSS/LIO**: positioning from GNSS/LiDAR integration using FGO.

(4) **GNSS/LIO GMM**: positioning from GNSS/LiDAR integration using FGO aided by GMM.

As the GNSS positioning only provides positional information, therefore, only 2 dimensions (2D) positioning performance is evaluated. The parameters used during the experiment are shown in Table I.

TABLE I. PARAMETER VALUES USED IN THIS PAPER

Window Size (M)	35 epochs
NDT Resolution	0.1
Component Num	3
NDT Step Size	0.1

B. Performance Evaluation of the Proposed Method in Urban Canyon

The positioning accuracy of the four compared methods is shown in Table II. A mean error of 7.01 meters is obtained using GNSS standalone positioning with a maximum error reaching up to 25.88 meters. Interestingly, the mean error for the LIO (12.86 meters) is even larger than the one for GNSS. Since the LIO estimates just the relative motion between consecutive frames, the error of LIO accumulates during the experiment. The tested challenging scene (Fig. 3) includes numerous moving vehicles which can significantly degrade the performance of LIO. The mean error is decreased to 5.51 meters by using the FGO-based GNSS/LIO. The application of the adaptive GMM reduces the mean error further to only 4.6 meters with a maximum error of 16.46 meters.

The resulting trajectories and translational are shown in Fig. 4 and Fig. 5, respectively. With the help of the adaptive GMM, the positioning error is reduced over large parts of the trajectory, compared with the conventional GNSS/LIO integration. Fig. 6 shows the amplification of selected details from the complete trajectory in Fig. 4. We can see these sections, that the results from GNSS/LIO with GMM (blue curve) always tends to be more smooth and closer to the ground truth trajectory than the conventional GNSS/LIO integration. This improvement is mainly caused by the adaptively modeling of GNSS using GMM.

Although the accuracy of GNSS/LIO integration is improved with the help of the proposed GMM, the remaining error is still about 4.5 meters. One reason for this is the fact that, with a mean error of 7 meters, the GNSS positioning accuracy is quite limited. Although the LIO can provide decent accuracy in a short period, the LIO cannot provide absolute positioning. In other words, the LIO can only help to smooth the trajectory instead of correcting the trajectory. We can see from Fig. 5 that the GNSS positioning peaks several times which means the environment conditions (e.g. satellite visibility) variate during the experiment. The error distribution for GNSS between epoch 250 and 350 is different from the one between 400 and 450 in Fig. 5 due to the environment change. Therefore, adaptively choosing the window size for estimating the GMM is significant. Currently, the window size is set as fixed (35 epochs). Therefore, this is another aspect that the proposed method can still be improved. One possible solution to cope with this is to employ the 3D building model to pre-determine the environment conditions. In future work, we will study the self-tuning of the window size for GMM.

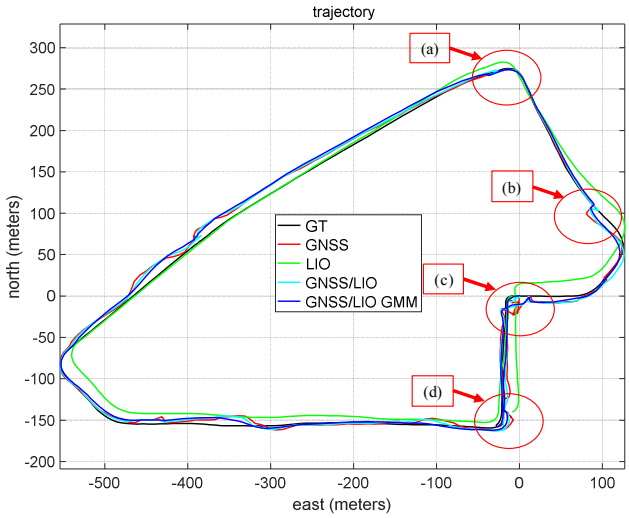

Fig. 4. Trajectories of the tested methods. The black curve denotes the ground truth trajectory from SPAN-CPT. The red and green curves denote the GNSS and LIO, respectively. The cyan and blue curves represent the GNSS/LIO integrations with and without GMM, respectively.

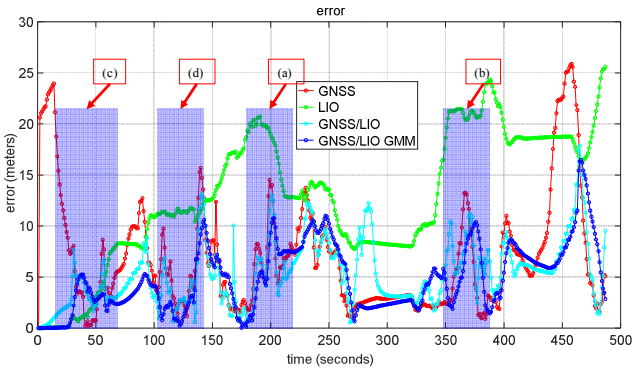

Fig. 5. Positioning errors of the tested methods. The red and green curves denote the GNSS and LIO, respectively. The cyan and blue represent the GNSS/LIO integrations with and without the GMM.

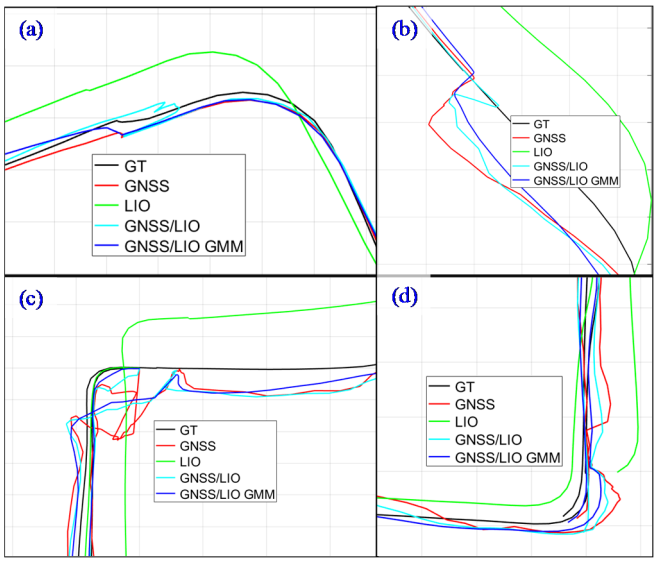

Fig. 6. The amplification of the trajectories in four selected portions with respect to Fig. 4.

TABLE II. POSITIONING PERFORMANCE OF THE EVALUATED METHODS

All data	GNSS	LIO	GNSS/LIO	GNSS/LIO GMM
Mean error	7.01 m	12.86 m	5.51 m	4.60 m
Std	5.73 m	6.39 m	3.19 m	3.33 m
Max error	25.88 m	25.62 m	17.86 m	16.46 m

C. *Discussion*

The parameter estimation of the GMM relies heavily on the residual of GNSS measurements. This section presents the residual and GNSS positioning error in east and north directions during the experiment, respectively. Fig. 7 shows the error and residual in the east direction. We can see from the blue histogram, which denotes the error, that the distribution has three peaks. In other words, three Gaussian components are needed to describe the error distribution during the experiment. The brown histogram denotes the residual over the experiment. The estimated residual can fit well regarding errors between [-5m, 5m]. However, the estimated residual cannot track the trend outside the bound of [-5m, 5m] well. This is due to the fact that the estimated residual relies heavily on the initial guess of the state estimation. If the estimated position deviates dramatically from the ground position, the residual cannot reflect the actual noise of GNSS measurements. Therefore, one drawback of the GMM is that it relies on the accuracy of the initial guess of the state estimation.

Fig. 8 shows the error and residual histograms in the north direction. There are also three peaks of the error as well as the residual. The peak on the left side in Fig. 8 deviates significantly from the zero. This is mainly due to the multipath and NLOS receptions which degrades the GNSS performance.

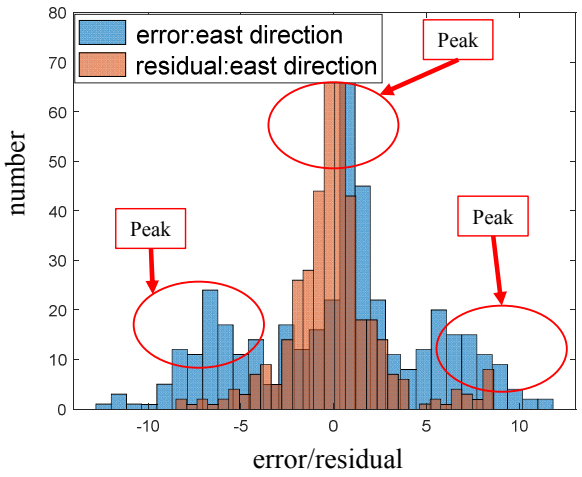

Fig. 7. The GNSS residual vs. error in the east direction during the experiment. The x-axis denotes the values of error or residuals. The y-axis represents the number of error or residual that belongs to a certain histogram.

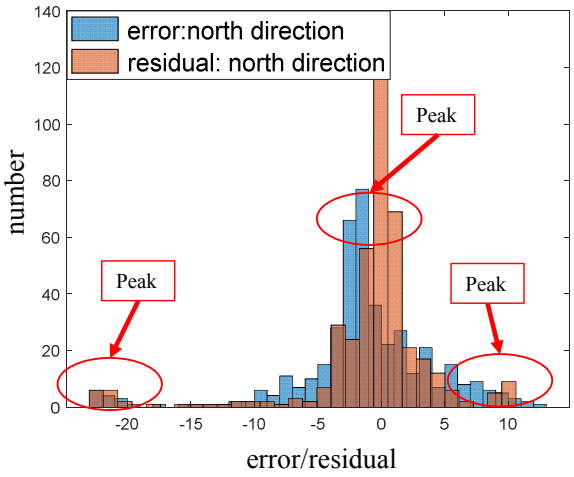

Fig. 8. The GNSS residual vs. error in the north direction during the experiment. The x-axis denotes the values of error or residuals. The y-axis represents the number of error or residual that belongs to a certain histogram.

VI. CONCLUSIONS AND FUTURE WORK

Effectively modeling the noise distribution of sensor measurements is significant for multi-sensor fusion, especially in challenging scenarios where the noise model variate dramatically. Instead of using a single Gaussian distribution, this paper explores to employ the GMM to describe the sensor measurement based on GNSS residuals. Improved performance is obtained with the help of GMM in GNSS/LIO integration. The proposed GMM can easily be adapted to other sensors, such as vision or radar. To enhance the sensitivity of the GMM against environmental change, we will utilize the recently developed context-awareness technique [39]. This could be a promising direction to further boost the robustness of the proposed method against environmental changes.

ACKNOWLEDGMENT

The authors acknowledge the support of the Hong Kong PolyU internal grant on the project ZVKZ, “Navigation for Autonomous Driving Vehicle using Sensor Integration”.

REFERENCES

[1] P. D. Groves, *Principles of GNSS, inertial, and multisensor integrated navigation systems*. Artech house, 2013.

[2] X. Lyu, H. Gu, Y. Wang, Z. Li, S. Shen, and F. Zhang, "Design and implementation of a quadrotor tail-sitter vtol uav," in *2017 IEEE international conference on robotics and automation (ICRA)*, 2017, pp. 3924-3930: IEEE.

[3] A. Geiger, P. Lenz, and R. Urtasun, "Are we ready for autonomous driving? the kitti vision benchmark suite," in *2012 IEEE Conference on Computer Vision and Pattern Recognition*, 2012, pp. 3354-3361: IEEE.

[4] L.-T. Hsu, "Analysis and modeling GPS NLOS effect in highly urbanized area," *GPS solutions,* vol. 22, no. 1, p. 7, 2018.

[5] T. Shan and B. Englot, "LeGO-LOAM: Lightweight and ground-optimized lidar odometry and mapping on variable terrain," in *2018 IEEE/RSJ International Conference on Intelligent Robots and Systems (IROS)*, 2018, pp. 4758-4765: IEEE.

[6] W. Wen, L.-T. Hsu, and G. J. S. Zhang, "Performance analysis of NDT-based graph SLAM for autonomous vehicle in diverse typical driving scenarios of Hong Kong," vol. 18, no. 11, p. 3928, 2018.

[7] A. Fernández *et al.*, "ATENEA: Advanced techniques for deeply integrated GNSS/INS/LiDAR navigation," in *2010 5th ESA Workshop on Satellite Navigation Technologies and European Workshop on GNSS Signals and Signal Processing (NAVITEC)*, 2010, pp. 1-8: IEEE.
[8] A. Shetty and G. X. Gao, "Covariance estimation for gps-lidar sensor fusion for uavs," in *Proceedings of the 30th International Technical Meeting of The Satellite Division of the Institute of Navigation (ION GNSS+ 2017), Portland, OR, USA*, 2017.
[9] D. Chen and G. X. Gao, "Probabilistic graphical fusion of LiDAR, GPS, and 3D building maps for urban UAV navigation," *Navigation,* vol. 66, no. 1, pp. 151-168, 2019.
[10] A. P. Shetty, "GPS-LiDAR sensor fusion aided by 3D city models for UAVs," 2017.
[11] W. Wen, G. Zhang, and L.-T. Hsu, "Object Detection Aided GNSS and Its Integration with LiDAR in Highly Urbanized Areas,," *IEEE Intelligent Transportation Systems Magazine (accepted),* p. Accepted, 2019.
[12] T. Pfeifer and P. Protzel, "Expectation-maximization for adaptive mixture models in graph optimization," in *2019 International Conference on Robotics and Automation (ICRA)*, 2019, pp. 3151-3157: IEEE.
[13] S. Hening, C. A. Ippolito, K. S. Krishnakumar, V. Stepanyan, and M. Teodorescu, "3D LiDAR SLAM integration with GPS/INS for UAVs in urban GPS-degraded environments," in *AIAA Information Systems-AIAA Infotech@ Aerospace*, 2017, p. 0448.
[14] S. J. A. M. Thrun, "Probabilistic algorithms in robotics," vol. 21, no. 4, pp. 93-93, 2000.
[15] F. Dellaert, M. J. F. Kaess, and T. i. Robotics, "Factor graphs for robot perception," vol. 6, no. 1-2, pp. 1-139, 2017.
[16] W. Wen, Y.-C. Kan, and L.-T. Hsu, "Performance Comparison of GNSS/INS Integrations Based on EKF and Factor Graph Optimization," presented at the ION GNSS+ 2019, Florida, 2019.
[17] F. Dellaert and M. Kaess, "Factor graphs for robot perception," *Foundations and Trends® in Robotics,* vol. 6, no. 1-2, pp. 1-139, 2017.
[18] L.-T. Hsu, Y. Gu, and S. Kamijo, "3D building model-based pedestrian positioning method using GPS/GLONASS/QZSS and its reliability calculation," *GPS solutions,* vol. 20, no. 3, pp. 413-428, 2016.
[19] P. D. Groves and M. J. G. S. Adjrad, "Likelihood-based GNSS positioning using LOS/NLOS predictions from 3D mapping and pseudoranges," vol. 21, no. 4, pp. 1805-1816, 2017.
[20] H.-F. Ng, G. Zhang, and L.-T. Hsu, "GNSS NLOS Pseudorange Correction based on Skymask for Smartphone Applications," presented at the ION GNSS+, 2019, Miami, Florida, USA, 2019.
[21] W. Wen, G. Zhang, and L.-T. Hsu, "Exclusion of GNSS NLOS receptions caused by dynamic objects in heavy traffic urban scenarios using real-time 3D point cloud: An approach without 3D maps," in *Position, Location and Navigation Symposium (PLANS), 2018 IEEE/ION*, 2018, pp. 158-165: IEEE.
[22] W. Wen, G. Zhang, and L.-T. Hsu, "Correcting GNSS NLOS by 3D LiDAR and Building Height," presented at the ION GNSS+, 2018, Miami, Florida, USA., 2018.
[23] W. Wen, G. Zhang, and L.-T. Hsu, "GNSS NLOS Exclusion Based on Dynamic Object Detection Using LiDAR Point Cloud," *IEEE Transactions on Intelligent Transportation Systems,* 2019.
[24] W. Wen, G. Zhang, and L. T. Hsu, "Correcting NLOS by 3D LiDAR and building height to improve GNSS single point positioning," *Navigation,* vol. 66, no. 4, pp. 705-718, 2019.
[25] X. Bai, W. Wen, and L.-T. Hsu, "Using Sky-Pointing Fish-eye Camera and LiDAR to Aid GNSS Single Point Positioning in Urban Canyons (submitted)," *IET Intelligent Transport Systems,* 2019.
[26] X. Bai, W. Wen, G. Zhang, and L.-T. Hsu, "Real-time GNSS NLOS Detection and Correction Aided by Sky-Pointing Camera and 3D LiDAR," presented at the Proceedings of ION Pacific PNT 2019, Honolulu, HA, USA, 2019.
[27] E. Olson and P. Agarwal, "Inference on networks of mixtures for robust robot mapping," *The International Journal of Robotics Research,* vol. 32, no. 7, pp. 826-840, 2013.
[28] D. M. Rosen, M. Kaess, and J. J. Leonard, "Robust incremental online inference over sparse factor graphs: Beyond the Gaussian case," in *2013 IEEE International Conference on Robotics and Automation*, 2013, pp. 1025-1032: IEEE.
[29] T. Pfeifer and P. Protzel, "Incrementally learned Mixture Models for GNSS Localization," *arXiv preprint arXiv:1904.13279,* 2019.
[30] T. Pfeifer and P. Protzel, "Robust sensor fusion with self-tuning mixture models," in *2018 IEEE/RSJ International Conference on Intelligent Robots and Systems (IROS)*, 2018, pp. 3678-3685: IEEE.
[31] R. M. Watson, J. N. Gross, C. N. Taylor, and R. C. Leishman, "Uncertainty Model Estimation in an Augmented Data Space for Robust State Estimation," *arXiv preprint arXiv:1908.04372,* 2019.
[32] R. M. Watson, J. N. Gross, C. N. Taylor, and R. C. Leishman, "Robust Incremental State Estimation through Covariance Adaptation," *arXiv preprint arXiv:1910.05382,* 2019.
[33] T. Stoyanov, M. Magnusson, H. Andreasson, and A. J. Lilienthal, "Fast and accurate scan registration through minimization of the distance between compact 3D NDT representations," *The International Journal of Robotics Research,* vol. 31, no. 12, pp. 1377-1393, 2012.
[34] N. Roy, P. Newman, and S. Srinivasa, "Inference on Networks of Mixtures for Robust Robot Mapping," 2013.
[35] J. Zhang and S. Singh, "LOAM: Lidar Odometry and Mapping in Real-time," in *Robotics: Science and Systems*, 2014, vol. 2.
[36] P. Biber and W. Straßer, "The normal distributions transform: A new approach to laser scan matching," in *Proceedings 2003 IEEE/RSJ International Conference on Intelligent Robots and Systems (IROS 2003)(Cat. No. 03CH37453)*, 2003, vol. 3, pp. 2743-2748: IEEE.
[37] S. Agarwal and K. Mierle, "Ceres solver," 2012.
[38] M. Quigley *et al.*, "ROS: an open-source Robot Operating System," in *ICRA workshop on open source software*, 2009, vol. 3, no. 3.2, p. 5: Kobe, Japan.
[39] H. Gao and P. D. Groves, "Context determination for adaptive navigation using multiple sensors on a smartphone," 2016: Institute of Navigation (ION).